XP-524 is a dual-BET/EP300 inhibitor that represses oncogenic KRAS and potentiates immune checkpoint inhibition in pancreatic cancer

Daniel R. Principe[a,b,1], Rui Xiong[c,1], Yangfeng Li[c], Thao N. D. Pham[d], Suneel D. Kamath[e], Oleksii Dubrovskyi[c], Kiira Ratia[c], Fei Huang[c], Jiong Zhao[c], Zhengnan Shen[c], Dinesh Thummuri[f], Zhou Daohong[f], Patrick W. Underwood[g], Jose Trevino[h], Hidayatullah G. Munshi[d,i], Gregory R. J. Thatcher[j,1,2], and Ajay Rana[b,i,1,2]

[a]Medical Scientist Training Program, University of Illinois College of Medicine, Chicago, IL 60612; [b]Department of Surgery, University of Illinois at Chicago, Chicago, IL 60612; [c]Department of Medicinal Chemistry and Pharmacognosy, University of Illinois at Chicago, Chicago, IL 60612; [d]Department of Medicine, Northwestern University Feinberg School of Medicine, Chicago, IL 60611; [e]Taussig Cancer Center, Cleveland Clinic, Cleveland, OH 44106; [f]Department of Pharmacodynamics, College of Pharmacy, University of Florida, Gainesville, FL 32610; [g]Department of Surgery, University of Florida College of Medicine, Gainesville, FL 32610; [h]Department of Surgery, Division of Surgical Oncology, Virginia Commonwealth University, Richmond, VA 23298; [i]Jesse Brown VA Medical Center, Chicago, IL 60612; and [j]Department of Pharmacology and Toxicology, College of Pharmacy, The University of Arizona, Tucson, AZ 85004

Edited by Michael Karin, Department of Pharmacology, Laboratory of Gene Regulation and Signal Transduction, University of California San Diego, La Jolla, CA; received September 11, 2021; accepted December 6, 2021

Pancreatic ductal adenocarcinoma (PDAC) is associated with extensive dysregulation of the epigenome and epigenetic regulators, such as bromodomain and extraterminal motif (BET) proteins, have been suggested as potential targets for therapy. However, single-agent BET inhibition has shown poor efficacy in clinical trials, and no epigenetic approaches are currently used in PDAC. To circumvent the limitations of the current generation of BET inhibitors, we developed the compound XP-524 as an inhibitor of the BET protein BRD4 and the histone acetyltransferase EP300/CBP, both of which are ubiquitously expressed in PDAC tissues and cooperate to enhance tumorigenesis. XP-524 showed increased potency and superior tumoricidal activity than the benchmark BET inhibitor JQ-1 in vitro, with comparable efficacy to higher-dose JQ-1 combined with the EP300/CBP inhibitor SGC-CBP30. We determined that this is in part due to the epigenetic silencing of KRAS in vitro, with similar results observed using ex vivo slice cultures of human PDAC tumors. Accordingly, XP-524 prevented KRAS-induced, neoplastic transformation in vivo and extended survival in two transgenic mouse models of aggressive PDAC. In addition to the inhibition of KRAS/MAPK signaling, XP-524 also enhanced the presentation of self-peptide and tumor recruitment of cytotoxic T lymphocytes, though these lymphocytes remained refractory from full activation. We, therefore, combined XP-524 with an anti–PD-1 antibody in vivo, which reactivated the cytotoxic immune program and extended survival well beyond XP-524 in monotherapy. Pending a comprehensive safety evaluation, these results suggest that XP-524 may benefit PDAC patients and warrant further exploration, particularly in combination with immune checkpoint inhibition.

pancreatic cancer | BET inhibitor | KRAS | PD-1

Pancreatic ductal adenocarcinoma (PDAC) is associated with uniformly poor clinical outcomes, in part because of incomplete responses to the standard of care chemotherapy. Accordingly, there is a need to better understand key molecular drivers of the neoplastic phenotype to identify new potential targets for therapy. Emerging evidence suggests that PDAC is associated with extensive dysregulation of the epigenome, particularly aberrant posttranslational histone modification (1). As such, a variety of epigenetic regulators have been suggested as potential drug targets in PDAC (2, 3), including bromodomain and extraterminal motif (BET) proteins, which appear to have several driving roles in PDAC pathobiology (4–7).

BET family members include the ubiquitously expressed BRD2, BRD3, and BRD4, as well as the testes-restricted BRDT. These proteins contain two tandem bromodomains (BD1 and BD2), an extraterminal domain, and a C-terminal domain (CTD), though BRD4 has an extended CTD with little sequence homology to other BET proteins (2, 8, 9). BET proteins recognize acetylated lysine residues via their bromodomains, acting as epigenetic readers and a wide variety of functions ranging from chromatin remodeling to transcriptional coactivation (10–12). In PDAC, BET proteins contribute to disease pathogenesis predominantly through the transcriptional activation of several oncogenes, including c-MYC and FOSL1 (5). Accordingly, BET inhibitors such as JQ-1 have shown preclinical efficacy in murine PDAC (4, 13). Given the mounting preclinical evidence supporting BET inhibitors in PDAC, clinicians have been eager to translate these findings to the bedside.

Accordingly, several BET inhibitors are currently being evaluated in clinical trials. Early reports seem to support the antitumor potential of BET inhibitors but also appear to suggest that their efficacy as single agents may be limited (2). Emerging

Significance

There are currently no effective treatments for pancreatic ductal adenocarcinoma (PDAC), which displays widespread resistance to chemotherapy, radiation therapy, and immunotherapy. Here, we demonstrate that the multispecificity BET/EP300 inhibitor XP-524 has pronounced single-agent efficacy in vitro, in vivo, and in ex vivo human PDAC slice cultures, functioning in part by attenuating oncogenic KRAS signaling. In vivo XP-524 led to extensive reprogramming of the pancreatic tumor microenvironment, sensitizing murine carcinoma to immune checkpoint inhibition and further extending survival. Given the urgent need for therapeutic approaches in PDAC, the combination of XP-524 and immune checkpoint inhibition warrants additional exploration.

Author contributions: D.R.P., G.R.J.T., and A.R. designed research; D.R.P., R.X., Y.L., T.N.D.P., O.D., K.R., F.H., J.Z., and Z.S. performed research; D.R.P., R.X., G.R.J.T., and A.R. analyzed data; R.X., Y.L., T.N.D.P., Z.S., D.T., Z.D., P.W.U., J.T., H.G.M., G.R.J.T., and A.R. contributed new reagents/analytic tools; and D.R.P., S.D.K., H.G.M., G.R.J.T., and A.R. wrote the paper.

The authors declare no competing interest.

This article is a PNAS Direct Submission.

[1]D.R.P., R.X., G.R.J.T., and A.R. contributed equally to this work.

[2]To whom correspondence may be addressed. Email: arana@uic.edu or grjthatcher@arizona.edu.

This article contains supporting information online at http://www.pnas.org/lookup/suppl/doi:10.1073/pnas.2116764119/-/DCSupplemental.

Published January 21, 2022.

data suggest that select BET inhibitors have increased efficacy when combined with the added inhibition of histone modifiers such as histone deacetylases (HDACs) (4). The rationale for combining HDAC and BET inhibitors stems from the established role of BET proteins as "acetylation scanners," as they accumulate on hyperacetylated chromatin regions at active promoters or enhancers (14). The redistribution of histone acetylation following HDAC inhibition alters the recruitment of BET proteins, delocalizing them from regulatory elements and directing them to new acetylated sites, thereby limiting their canonical effects on transcription (15).

However, it is important to note that HDAC inhibitors do not eliminate aberrant histone acetylation in cancer and instead redirect it. As histone acetyltransferases (HATs) are directly responsible for histone acetylation, we hypothesized that HAT inhibition might have a more dramatic effect on conferring BET inhibitor sensitivity. Perhaps the best-studied HAT is the EP300, one of several non-BET, bromodomain-containing proteins (16–18). The EP300 bromodomain serves important roles in mediating chromatin remodeling and gene activation (16–18). Additionally, the EP300 bromodomain is essential for oncogenic cMYC expression and cell proliferation (19). Hence, emerging evidence supports the therapeutic inhibition of EP300 (and its structural analog CBP) in multiple myeloma (20), and the combination EP300 inhibition and the BET inhibitor JQ-1 is showing early preclinical promise in a variety of tumor types (21, 22). However, inhibitors of EP300 have yet to enter a clinical trial, and EP300 inhibition has yet to be evaluated in combination with additional BET inhibitors in any sold tumor.

To address this, our group has recently synthesized the compound XP-524 (23), designed to simultaneously target the bromodomains of BRD4 and EP300/CBP. After verifying the selectivity and potency of this compound, we conducted several in vitro studies affirming that XP-524 has improved efficacy compared to the benchmark BET inhibitor JQ-1 and comparable efficacy to high-dose JQ-1 combined with EP300/CBP inhibition. This was confirmed through RNA sequencing, which determined that XP-524 significantly represses tumor-permissive KRAS signaling in vitro, which was also observed when cells were treated with the combination of JQ-1 and an EP300/CBP inhibitor. XP-524 showed significant, single-agent efficacy in the Ptf1a-Cre × LSL-$Kras^{G12D}$ (KC) model of early neoplastic disease, the Pdx1-Cre × LSL-$Kras^{G12D}$ × LSL-$TP53^{R172H\pm}$ (KPC) model of advanced PDAC, and the Pdx1-Cre × LSL-$Kras^{G12D}$ × LSL-$TP53^{R172H+/+}$ (KPPC) model of hyperaggressive PDAC.

In addition to extending survival in models of invasive PDAC, XP-524 enhanced tumor accumulation of T lymphocytes. However, these T lymphocytes remained refractory from full activation, demonstrating high expression of T cell exhaustion marker PD-1 and limited production of IFNγ and perforin. As XP-524 also enhanced the antigen presentation via major histocompatibility complex (MHC) class I and attenuated transforming growth factor β (TGFβ) biosynthesis, both barriers to the efficacy of PD-1 inhibition in PDAC (24, 25), we then combined XP-524 with an anti–PD-1 antibody in vivo. In addition to enhancing survival well beyond XP-524 in monotherapy, the combination of XP-524 and anti–PD-1 antibody further increased the recruitment of cytotoxic T lymphocytes, now highly active for cytotoxic surrogates IFNγ and perforin. Combined, these results suggest that XP-524 may have utility in the treatment of PDAC, reshaping the pancreatic tumor microenvironment and conferring sensitivity to immune checkpoint inhibition.

Results

BRD4 and EP300/CBP Are Ubiquitously Expressed in PDAC. To determine the potential for a multispecificity BRD4/EP300 inhibitor in PDAC, we first evaluated the expression of both proteins in a cohort of human PDAC excisional biopsies (n = 14) and adjacent nonmalignant tissue (n = 9). In addition to an increase in staining intensity, PDAC tissues had a comparative increase in the percent of nuclei positive for both BRD4 and EP300/CBP when compared to adjacent nonmalignant specimens (Fig. 1 *A* and *B*). Similarly, both *BRD4* and *EP300* messenger RNA (mRNA) expression were increased in PDAC tumor specimens when compared to adjacent, nonmalignant tissues in two publicly available genomic datasets (Fig. 1 *C* and *D*). BRD4 and EP300/CBP were ubiquitously expressed in PDAC cell lines (Fig. 1*E*) and displayed a similar pattern of nuclear localization in Panc1 cells, with exclusively nuclear expression of BRD4 and a combination of nuclear and cytoplasmic expression of EP300/CBP (Fig. 1*F*).

We next evaluated the expression of BRD4 and EP300/CBP in the pancreata of increasingly aggressive mouse models of PDAC by immunohistochemistry (IHC). We observed a modest increase in nuclear accumulation of BRD4 and EP300/CBP in the KC model of early disease, which localized predominantly to developing pancreatic, intraepithelial, pancreatic epithelial neoplasms (PanINs). We found stronger, uniform nuclear expression of both proteins in tumor tissue from the KPC model of invasive PDAC, as well as that of the KPPC model of extremely aggressive PDAC and the G-68 primary cell line–derived xenograft (CDX) model (Fig. 1*G* and *SI Appendix*, Fig. S1 *A* and *B*).

XP-524 Is a Potent Multispecificity BET Inhibitor that Engages BRD4 and EP300/CBP. Given the conserved expression patterns of BRD4 and EP300/CBP in PDAC tissues, we next explored the potential of the novel compound XP-524 (23) as a dual-specificity inhibitor targeting the bromodomains of BRD4 and EP300/CBP (Fig. 2*A*). This compound showed superior potency compared to the prototypical, benchmark BET inhibitor JQ-1 by time-resolved fluorescence energy transfer (TR-FRET) assay: XP-524 half-maximal inhibitory concentration (IC_{50}) = 5.8 (BRD4-BD1) and 1.5 nM (BRD4-BD2); JQ-1 IC_{50} = 200 (BRD4-BD1) and 114 nM (BRD4-BD2) (Fig. 2 *B* and *C*). Further analysis via the alternative BROMOscan assay confirmed that XP-524 binds strongly to and inhibits EP300 and CBP proteins with an IC_{50} of 28 and 116 nM, respectively (Fig. 2*D*).

To verify the binding of XP-524 to its target proteins and explain the observed multispecificity, we acquired cocrystal structures of XP-524 in complex with the bromodomains of BRD4 and the EP300 homolog CBP (CBP providing favorable solubility characteristics over EP300 for cocrystallization). We found that XP-524 similarly orients itself in both the BRD4-BD1 and the CBP bromodomain, making extensive contacts at the acetylated lysine pocket (Fig. 2*E*). The pyrrolopyridone group of XP-524 forms a bidentate hydrogen-bonding interaction with Asn-1168 in the CBP bromodomain, and the sulfate moiety inserts itself into the ZA loop and forms a hydrogen bond with the backbone of Asp-1116. The indole scaffold fits snugly into the LPF shelf through hydrophobic interactions (Fig. 2*F*).

An overlay of the XP-524–CBP complex with the XP-524–BRD4 complex demonstrated similar binding modes. The bottom pyridine ring of the CBP complex rotates 90°, as CBP lacks the Trp for a pi–pi interaction in the LPF pocket. However, XP-524 forms a cation–pi interaction with Arg-1173, a key interaction in the design of potent EP300/CBP inhibitors (26–28). Contrastingly, JQ-1 is not able to capture this important cation–pi interaction, as the chlorophenyl ring of JQ-1 clashes with Arg-1173, thereby blocking the binding of JQ-1 to CBP and the ability of JQ-1 to act as an EP300/CBP inhibitor (Fig. 2*G*).

XP-524 Disrupts Oncogenic KRAS Signaling In Vitro and Ex Vivo. To explore the potential utility of the XP-524 compound in pancreatic cancer cells, we first incubated an equal number of Panc1 tumor cells with either a DMSO vehicle, 1 μM JQ-1, 1 μM of the EP300/CBP inhibitor SGC-CBP30, JQ-1 and SGC-CBP30,

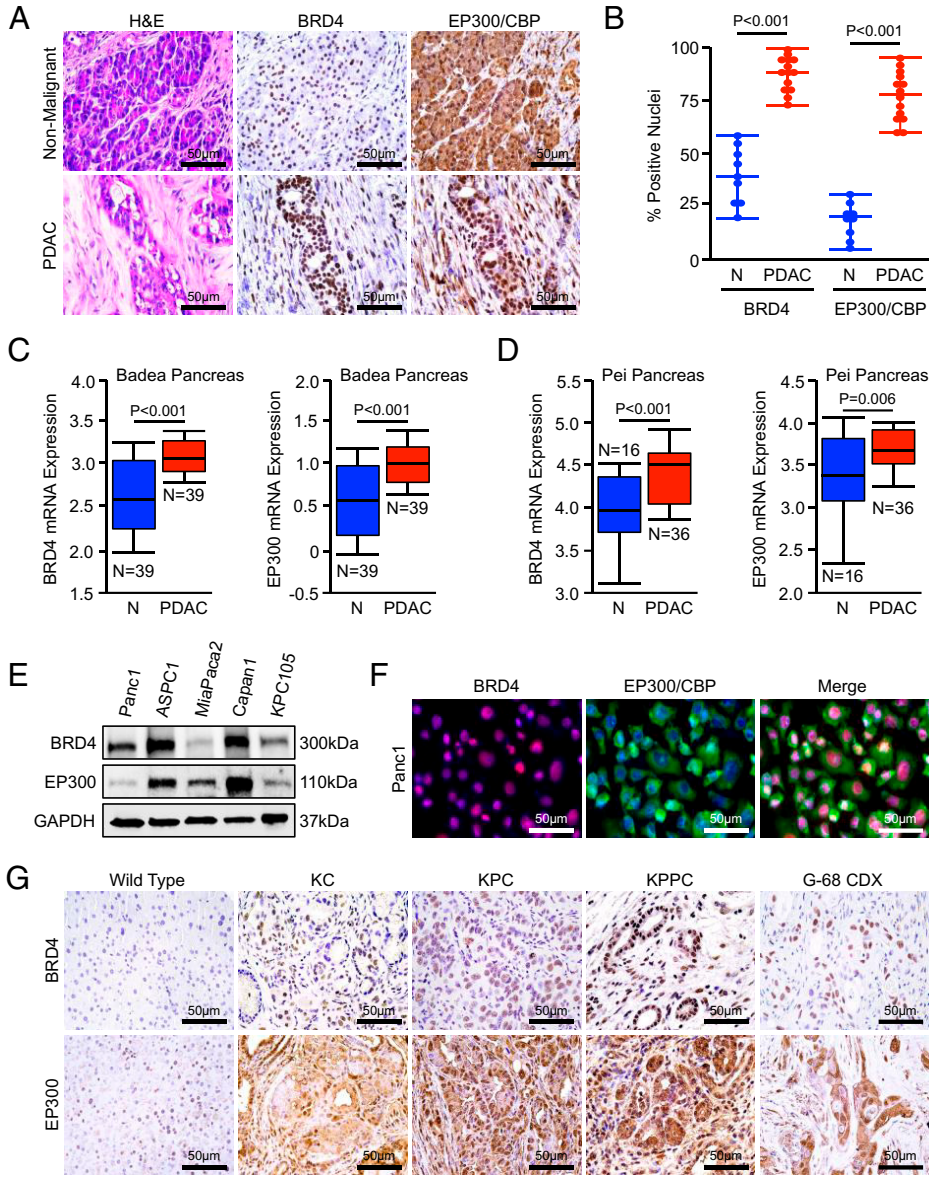

Fig. 1. BRD4 and EP300/CBP are ubiquitously expressed in PDAC. (*A* and *B*) Excisional biopsies from 14 PDAC patients, nine with matched, adjacent nonmalignant tissue, were sectioned and stained for either BRD4 or EP300/CBP. The number of positive nuclei per 40× field was quantified by three blinded investigators and divided by the total number of nuclei in each field. These values were averaged and displayed as an individual value plot. (*C* and *D*) Pancreatic tumor tissues (PDAC) and adjacent nonmalignant (N). The Badea et al. and Pei et al. cohorts of PDAC patients were evaluated for mRNA expression of *BRD4* or *EP300* using the Oncomine platform. All mRNA expression values are plotted in log scale. (*E*) Human PDAC cell lines Panc1, ASPC1, MiaPaCa2, Capan1, and the murine PDAC cell line KPC-105 were evaluated for expression of BRD4 and EP300/CBP by Western blot. (*F*) Panc1 cells were stained for BRD4 and EP300/CBP by immunocytochemistry. (*G*) Pancreas tissue from either nongenic wild type, the KC model of PanIN disease, the KPC model of advanced PDAC, the KPPC model of extremely aggressive PDAC, or subcutaneous tumor tissue from the G-68 CDX model were collected and stained for either BRD4 or EP300/CBP.

and 1 μM XP-524 or XP-524 and SGC-CBP30 and monitored cell growth kinetics until DMSO-treated cells reached 100% confluence. While JQ-1 led to modest growth suppression, this was markedly enhanced by the addition of SGC-CBP30, though SGC-CBP30 had a marginal effect on cell growth without JQ-1 (Fig. 3*A* and *SI Appendix*, Fig. S2*A*). Contrastingly, XP-524 was highly effective at suppressing tumor cell growth, closely resembling the combined effects of JQ-1 and SGC-CBP30. Consistent with its role as an EP300/CBP inhibitor, the effect of XP-524 was not further enhanced by the addition of SGC-CBP30 (Fig. 2*A*).

After repeating this experiment using MiaPaCa2 and ASPC1 cells (*SI Appendix*, Fig. S2 *B* and *C*), we next incubated Panc1 cells with increasing concentrations of either JQ-1 or XP-524, with or without a fixed 1-μM dose of SGC-CBP30. After 48 h, we examined changes in cell viability via 3-(4,5-Dimethyl-2-thiazolyl)-2,5-diphenyl-2H-tetrazolium bromide (MTT) assay. Similar to the effects observed on cell growth, the reduction in cell viability by JQ-1 was enhanced by the addition of SGC-CBP30, significantly reducing the observed IC_{50}. While the combination of JQ-1 and SGC-CBP30 was similar in maximum efficacy to XP-524, XP-524 was more effective at lower concentrations and again unaffected by the addition of SGC-CBP30 (Fig. 3*B* and *SI Appendix*, Fig. S2*D*).

To identify the cellular mechanisms that underlie these changes, we next incubated Panc1 tumor cells with either a DMSO vehicle, JQ-1, JQ-1, and SGC-CBP30 or XP-524. After 24 h, cells were subjected to RNA sequencing (Fig. 3*C*). Post hoc gene set enrichment analysis (GSEA) suggested that XP-524 most significantly suppresses oncogenic KRAS signaling, as well as several associated cellular processes, including the MAPK pathway and cell cycle progression (Fig. 3 *D* and *E*). While JQ-1 led to modest suppression of KRAS and cell cycle pathways, this was potentiated by the addition of SGC-CBP30, though less than the effects observed using XP-524 (Fig. 3 *D* and *E*). Given the suggested effects of XP-524 on in *KRAS* mRNA by RNA sequencing, we next treated Panc1 cells as described and evaluated *KRAS* expression after 6 h by qPCR. This affirmed a highly significant reduction in KRAS transcription following treatment with XP-524 (Fig. 3*F*), which was also observed using MiaPaCa2 and ASPC1 cells (Fig. 3 *G* and *H*).

We then retreated Panc1 cells with JQ-1, JQ-1 and SGC-CBP30, or XP-524 assessed alterations in protein expression by Western blot. While JQ-1 and JQ-1/SGC-CBP30 modestly

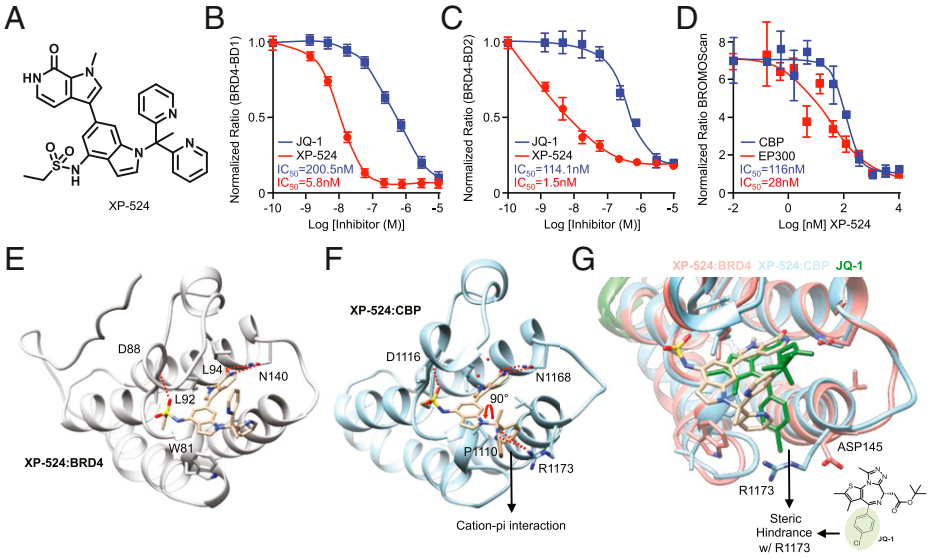

Fig. 2. XP-524 is a potent, multispecificity BET inhibitor that engages BRD4 and EP300/CBP. (*A*) Chemical structure of XP-524, designed to function as a multispecificity BET inhibitor with activity against EP300/CBP. (*B* and *C*) TR-FRET assay using either the first (BD1) or second (BD2) bromodomain of BRD4 and increasing concentrations of either the first-generation BET inhibitor JQ-1 or XP-524. (*D*) BROMOscan assay using EP300 or its structural analog CBP and increasing concentrations of XP-524. (*E*) Cocrystal structure of XP-524:BRD4, showing extensive interactions between XP-524 and the acetylated lysine pocket of the BD1 bromodomain (PDB: 6P05). (*F*) Cocrystal structure of XP-524 with EP300 analog CBP (XP-524:CBP), showing extensive interactions between XP-524 and the acetylated lysine pocket of the CBP bromodomain, as well as bidentate hydrogen bonding with Asn-1168 and the insertion of the sulfate moiety into the ZA loop forming a hydrogen bond with the backbone of Asp-1116 (PDB: 7JUO). (*G*) Overlay of the XP-524-CBP complex and the XP-524-BRD4 complex showing a similar binding mode.

reduced coprecipitation of BRD4 and EP300/CBP, compared to controls, this was nearly absent in cells incubated with XP-524 (Fig. 3*I*). This was associated with a significant reduction in KRAS expression as well as MEK/ERK activation following XP-524 treatment, paralleled by reductions in phosphorylated RB. Interestingly, JQ-1 treatment seemingly caused a compensatory increase in histone acetylation using H3K27ac as a surrogate marker, which was ameliorated with the addition of SGC-CBP30 and not observed in XP-524–treated cells (Fig. 3*J*). Using these same lysates, we also evaluated the association between BRD4 and EP300/CBP by immunoprecipitation. We next repeated this experiment using the primary KPC-105 murine PDAC cell line, which also demonstrated significant, XP-524–induced suppression of KRAS expression and inhibition of downstream MEK/ERK activation, with similar results observed regarding RB phosphorylation and H3K27 acetylation (Fig. 3K). In more abbreviated experiments, XP-524 led to similar reductions in KRAS protein expression and downstream MEK/ERK activation in MiaPaCa2 and ASPC1 cells (Fig. 3*L*).

Given the inherent limitations of two-dimensional cell culture, we next established primary PDAC slice cultures (Fig. 3M) by extracting 6-mm cores from resection specimens from three patients, sectioning cores at 250-μm intervals, and culturing ex vivo as described (29, 30). Slice cultures were incubated with either a DMSO vehicle or XP-524 (5 μM) and evaluated after 72 h by IHC. Consistent with our in vitro data (Fig. 3*J*), XP-524 significantly reduced ERK activation in human PDAC slice cultures, as well as cell proliferation in CK19+ tumor epithelial cells (Fig. 3 *N*–*P*).

XP-524 Reduces Mutant KRAS-Induced PanIN Formation In Vivo. Given the effects of XP-524 on disrupting oncogenic KRAS signaling in vitro, we next sought to determine whether XP-524 would similarly restrain KRAS-mediated oncogenesis in vivo. We, therefore, used the well-established KC model of neoplastic disease. This model serves as a reliable representation of early carcinogenesis, developing PanINs at 8 wk that do not typically progress to invasive carcinoma (31, 32). This is well-represented in our colony, in which KC mice are maintained in a full C57/B6 background and develop focal areas of PanIN disease at 8 wk with 100% penetrance, which continue to develop throughout the pancreas with less than 5% of mice developing focal PDAC at 1 y of age.

Using these mice, we first conducted a chemoprevention study in which 8-wk-old KC animals were randomized at a 50:50 male to female ratio into one of two treatment groups. Mice were administered daily intraperitoneal (IP) injections of either a phosphate-buffered saline (PBS) vehicle or 5 mg/kg XP-524 and killed at a fixed time point of 6 mo (Fig. 4*A*). Tissues were collected at the study end point, and mice treated with XP-524 showed a consistent reduction in the weight of the pancreas, particularly when normalized to total body weight (Fig. 4*B*). On histologic evaluation, XP-524–treated mice showed a significant reduction in lesion burden and fibrosis, as well as increased preservation of normal acinar tissue (Fig. 4 *C* and *D*). Similar to results in cell culture systems, XP-524–treated mice had a substantial reduction in expression of the mutant RAS protein by IHC, paralleled by reductions in ERK activation and cell proliferation (Fig. 4 *E* and *F*). This was also observed by Western blotting, in which XP-524–treated mice had a consistent reduction in KRAS expression, as well as downstream activation of MEK/ERK signals (Fig. 4*G*).

XP-524 Extends Survival and Inhibits KRAS Signaling in Murine PDAC. To explore the efficacy of XP-524 in advanced disease, we next utilized two transgenic models of pancreatic carcinogenesis, the first being the KPC model of invasive PDAC (33). This model closely mimics human PDAC histotypes and develops the full spectrum of disease ranging from early PanINs to invasive PDAC (33). Using these mice, we first conducted an early intervention study in which animals were allowed to develop overt PDAC for 15 wk, the point at which KPC mice in our colony develop focal PDAC with 100% penetrance (25). At this time, mice were randomized at a 50:50 male to female ratio into one of two treatment groups (n = 7 per group). Mice were administered daily IP injections of either a PBS vehicle or 5 mg/kg XP-524 and killed when showing clear signs of health decline (Fig. 5*A*). Interestingly, XP-524 significantly delayed mortality in KPC mice, extending median survival from 43- to 108-d postenrollment (Fig. 5*B*). Tissues were collected at the study end point, sectioned, and stained either with hematoxylin and eosin (H&E), trichrome, or IHC for pERK. Consistent with our in vitro results, XP-524–treated mice had substantially

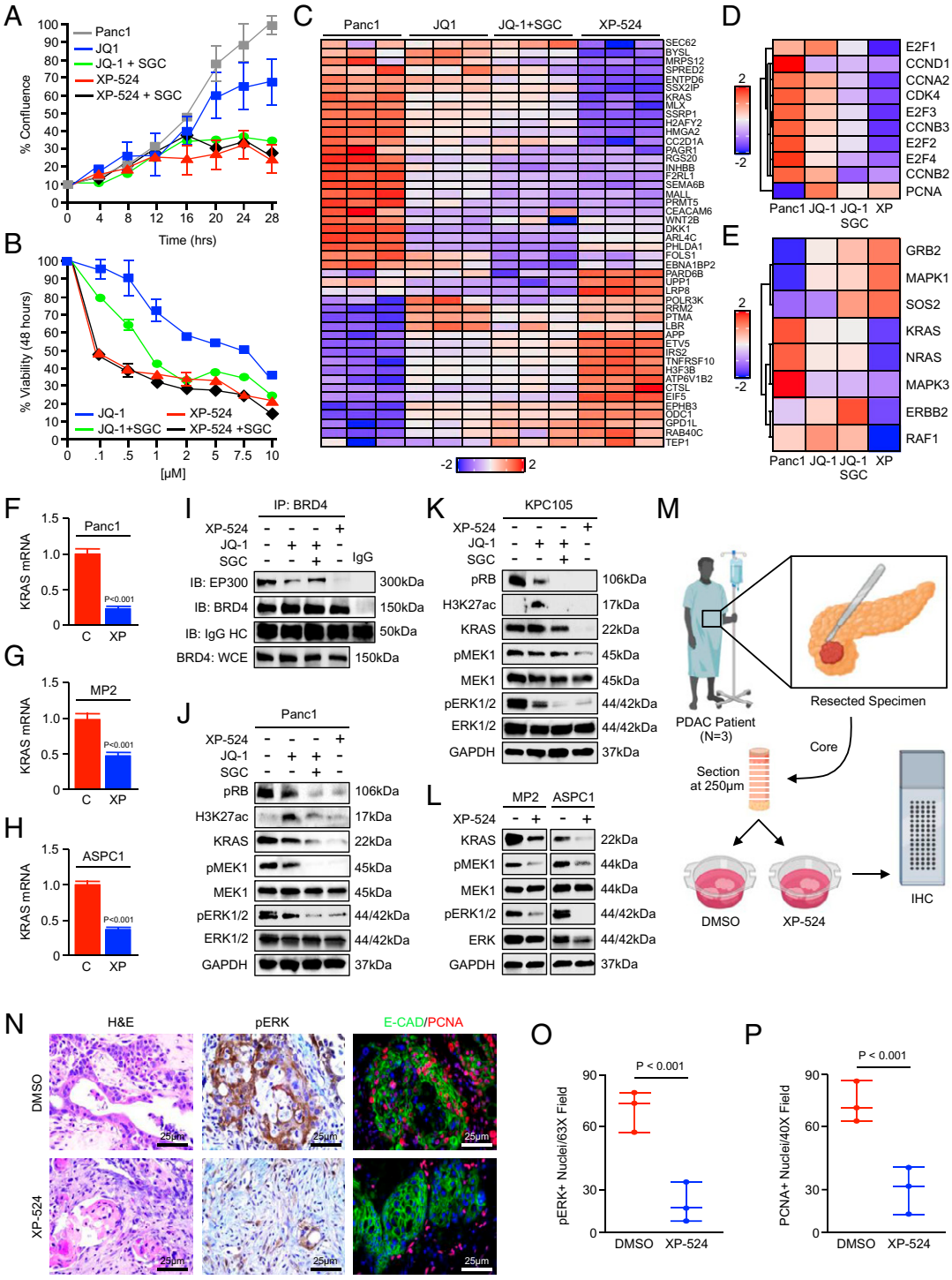

Fig. 3. Inhibition of EP300/CBP potentiates BETi-mediated silencing of oncogenic KRAS signaling. (*A*) An equal number of Panc1 cells were seeded in 24-well plates and treated with either a DMSO vehicle, 1 μM JQ-1, JQ-1 and 1 μM SGC-CBP30, 1 μM XP-524, or XP-524 and SGC-CBP30. Cell growth was evaluated every 4 h until the control group reached 100% confluence ($n = 4$ per group). (*B*) Panc1 cells were incubated with increasing concentrations of either JQ-1 or XP-524, each with or without a fixed 1-μM dose of SGC-CBP30. After 48 h, cell viability was evaluated by MTT assay. (*C*) Panc1 cells were incubated with either a DMSO vehicle, 1 μM JQ-1, JQ-1, and 1 μM SGC-CBP30, or 1 μM XP-524 and subjected to RNA sequencing. (*D*) Focused heatmap showing select, significantly altered genes in the cell cycle pathway using a false discovery rate (FDR)–adjusted *P* value of <0.05. (*E*) Focused heatmap showing select, significantly altered genes in the KRAS signaling pathway using an FDR-adjusted *P* value of <0.05. (*F–H*) Panc1, MiaPaCa2 (MP2), and ASPC1 cells were treated with 1 μM XP-524 and KRAS mRNA evaluated by qPCR. Values are presented as fold change compared to DMSO control (C)-treated samples. (*I*) Panc1 cells were again treated with 1 μM JQ-1, JQ-1 and 1 μM SGC-CBP30, or 1 μM XP-524 and the interaction between BRD4 and EP300 evaluated by immunoprecipitation (IP) followed by Western blot (IB). (*J* and *K*) Panc1 and KPC-105 cells were treated as described and evaluated by Western blot for pRB, H3K27 acetylation, as well as KRAS expression and downstream activation of the MEK/ERK pathway. (*L*) MiaPaCa2 (MP2) and ASPC1 cells and KRAS expression and downstream MEK/ERK activation evaluated by Western blot. (*M–P*) Excisional biopsies from three PDAC patients undergoing survival resection were cored, sectioned at 250-μm interval, and cultured ex vivo either in a control PBS vehicle or 5 μM XP-524. After 72 h, slice cultures were formalin fixed, paraffin embedded, and stained with H&E or by IHC for pERK or CK19 and PCNA.

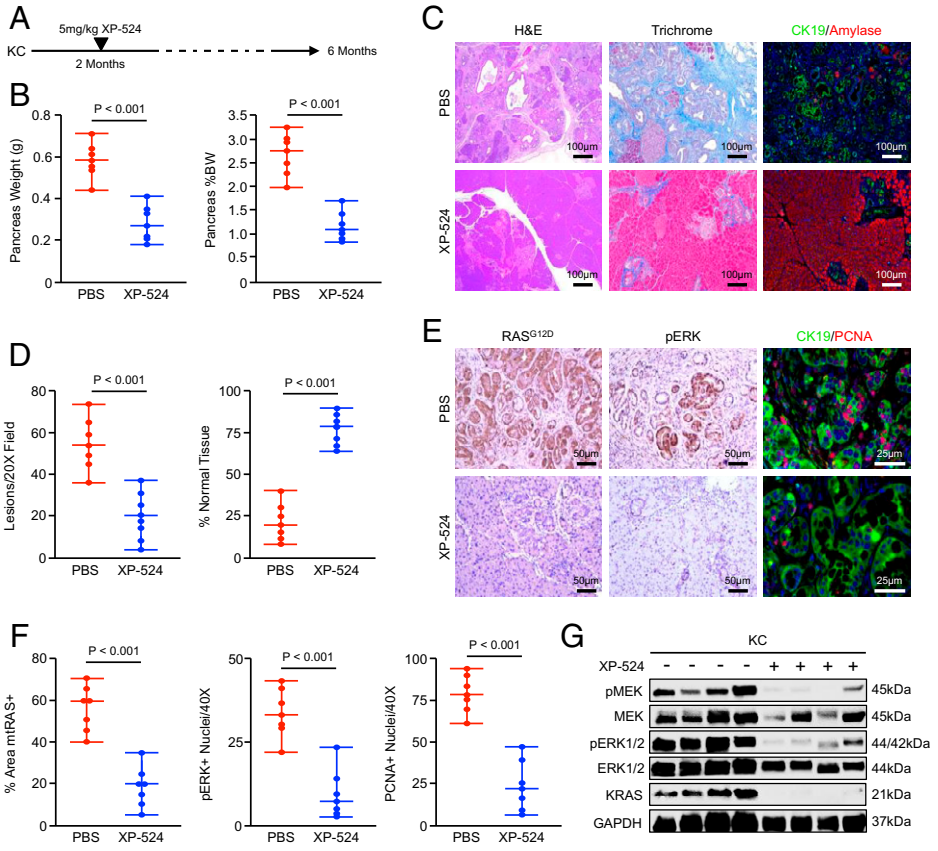

Fig. 4. XP-524 reduces mutant KRAS-induced PanIN formation in vivo. (*A*) KPC mice were generated as a model of early PanINs. Starting at 8 wk of age, mice were administered daily IP injections of either PBS vehicle or 5 mg/kg XP-524 and killed at a fixed end point of 6 mo. (*B*) At the study end point, the pancreas gland was weighted, normalized to each animal's body weight, and results displayed as individual value plots. (*C* and *D*) Pancreas tissues were stained with H&E, Masson's Trichrome, or via IHC for CK19 and pancreatic amylase, quantified as described, and results displayed as individual value plots. (*E* and *F*) Tissues were also stained by IHC for mutant RAS^{G12D}, pERK, or CK19 and PCNA. Results were quantified as described and displayed as individual value plots. (*G*) Pancreas tissues were lysed at the study end point and evaluated by Western blot for KRAS expression and downstream activation of the MEK/ERK pathway.

reduced ERK activation, with parallel reductions in cell proliferation and uniform increases in apoptosis (Fig. 5 *C* and *D*).

We next conducted a late intervention study using the KPPC model of extremely aggressive PDAC. In our colony, KPPC mice have a median survival of 43 d (n = 12) and develop extensive PDAC as early as 2 wk of age. We, therefore, enrolled mice as described either when they developed a 0.5-cm tumor or at 4 wk of age and placed them into one of two treatment groups (n = 6 per group). As previously described, mice were administered daily IP injections of either a PBS vehicle or 5 mg/kg XP-524 and killed when showing clear signs of health decline (e.g., weight loss, ascites, or lethargy) (Fig. 5*E*). As in KPC mice, XP-524 delayed mortality in KPPC mice, extending median survival from 23- to 50-d postenrollment (Fig. 5*F*). At the study end point, tissues were stained either with H&E or by IHC, which revealed a modest reduction in tumor stroma and a significant decrease in ERK activation and a subsequent increase in apoptosis (Fig. 5 *G* and *H*).

XP-524 Enhances T Cell Recruitment but Fails to Promote a Functional Antitumor Immune Response. Beyond the described changes in mitosis and ERK activation, we also observed substantial changes in tumor architecture following treatment with XP-524. When compared to the KPC control group, XP-524–treated tumors had a highly cellular stroma, hallmarked by a consistent increase in lymphocyte infiltration, the majority of which stained positive for the T cell marker CD3 and was confined to the tumor edge (Fig. 6*A*). However, these T cells were largely positive for the exhaustion markers/inhibitory checkpoint molecules, PD-1, CTLA-4, and VISTA, and XP-524–treated tumors stained negatively for the surrogate marker of cytotoxicity granzymeB (Fig. 6*B* and *SI Appendix*, Fig. S3*A*). To better evaluate the immune infiltrate, we repeated our in vivo study, enrolling KPC mice as described and treating them for a fixed, 2-mo period. At the study end point, the pancreata and spleens from PBS- and XP-524–treated mice (n = 4 per group) were harvested and subjected to flow cytometry.

Consistent with the prior histopathology, tumors from XP-524–treated mice displayed a significant increase in the infiltration of both CD4+ and CD8+ T cells (Fig. 6*C*), though there was no significant difference observed in the spleen (*SI Appendix*, Fig. S3*B*). However, when compared to positive controls, these intratumoral CD8+ T cells were negative for the activation surrogate IFNγ (Fig. 6*D*), and both CD4+ and CD8+ T cells were largely positive for PD-1 (Fig. 6*E*). Interestingly, XP-524–treated mice had a significant reduction in the relative abundance of intratumoral CD4+CD25+FoxP3+ regulatory T cells (Tregs) (Fig. 6*F*), though this was not observed in the spleen (*SI Appendix*, Fig. S3*B*). Mice treated with XP-524 had no consistent increase in CD45+CD11b+GR-1+ macrophage infiltration, though we observed a modest decrease in expression of the M2 surrogate CD206 (*SI Appendix*, Fig. S3*C*).

To further explore mechanisms of XP-524–associated alterations in tumor immunogenicity, we revisited our previous RNA-sequencing data in Panc1 cells and explored cell processes related to immune cell processes. Using this approach, we found that XP-524 led to up-regulation of the antigen-processing/presentation pathway (Fig. 6*G*), significantly increasing the mRNA expression of a variety of human leukocyte antigen molecules (Fig. 6*H*). This was also observed in vivo, in which XP-524–treated mice demonstrated increased surface staining for MHC Class 1 (Fig. 6*I*). RNA-sequencing data also identified a pronounced suppression of the TGFβ pathway (Fig. 6 *J* and *K*). We, therefore, evaluated the concentration of TGFβ1 by enzyme-linked immunosorbent assay (ELISA) and found that KPC mice treated with XP-524 displayed reduced

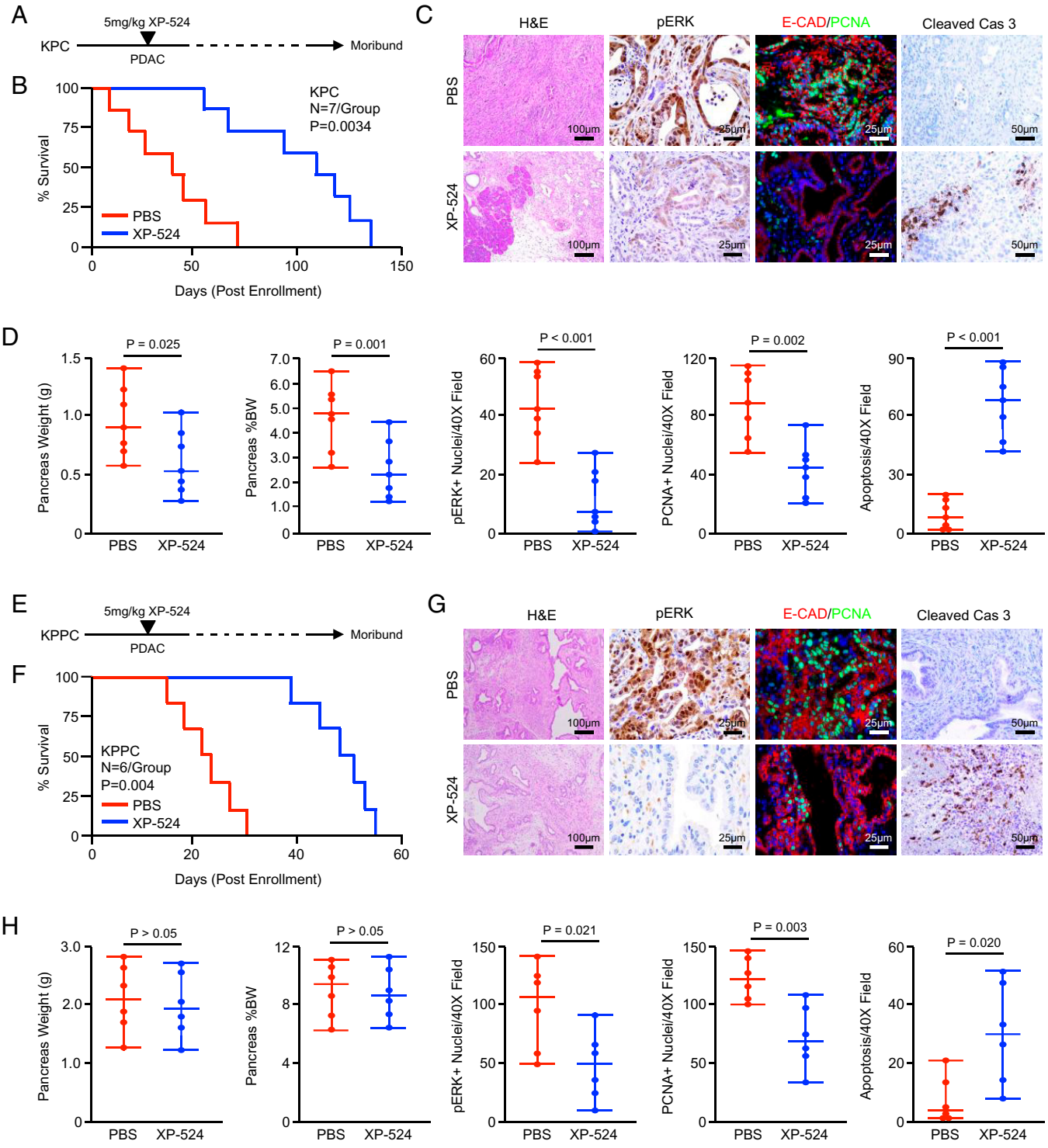

Fig. 5. XP-524 extends survival and reduces pathologic KRAS activation in murine PDAC. (*A*) KPC mice were generated as a model of advanced PDAC. Starting at 15 wk of age, mice were administered daily IP injections of either PBS vehicle or 5 mg/kg XP-524. Pancreas tissues were collected when the animals were moribund. (*B*) Kaplan–Meier curve indicating survival for mice across both groups in days postenrollment ($n = 7$ per group). (*C* and *D*) At the study end point, gross changes in pancreas gland structure were evaluated, including gland weight, which was also normalized to each animal's body weight, and results displayed as individual value plots. Tissues were stained with H&E or via IHC for pERK, E-cadherin and PCNA, or cleaved caspase 3, quantified as described, and results displayed as individual value plots. (*E*) KPPC mice were generated as a model of extremely aggressive PDAC. Mice were enrolled either at 2 wk of age or when developing a 0.5-cm^3 tumor. (*F*) Kaplan–Meier curve indicating survival for mice across both groups in days postenrollment ($n = 6$ per group). (*G* and *H*) At the study end point, gross changes in pancreas gland structure were evaluated, including gland weight, which was also normalized to each animal's body weight, and results displayed as individual value plots. Tissues also were stained with H&E or via IHC for pERK, E-cadherin, and PCNA or cleaved caspase 3, quantified as described, and results displayed as individual value plots.

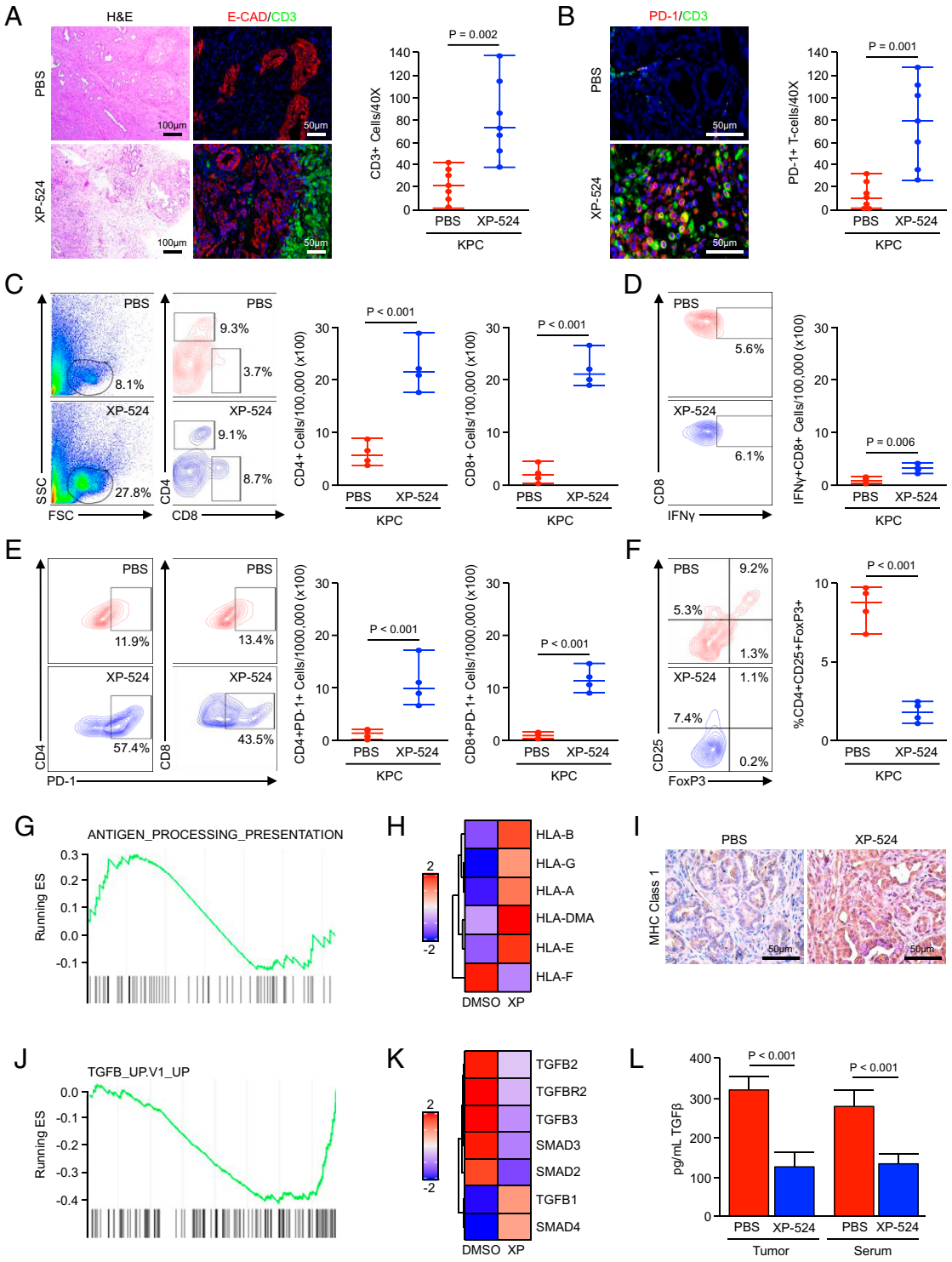

Fig. 6. XP-524 enhances T cell recruitment but fails to promote a functional antitumor immune response. (*A* and *B*) KPC mice were generated as a model of advanced PDAC. Starting at 15 wk of age, mice were administered daily IP injections of either PBS vehicle or 5 mg/kg XP-524. Pancreas tissues were collected when the animals were moribund and stained with either H&E or via IHC for E-cadherin and the T cell surrogate CD3 or for CD3 and T cell exhaustion marker PD-1. Tissue sections were quantified as described and displayed as an individual value plot. (*C*) KPC were enrolled as described and treated with either a PBS vehicle or 5 mg/kg XP-524. After 2 mo on treatment, tumor tissues were collected and analyzed by flow cytometry for tumor-infiltrating CD4+ and CD8+ T cells, respectively ($n = 4$ per group). FSC, forward scatter; SSC, side scatter. (*D*) Tumor-infiltrating cells were gated based on the CD8 staining shown previously, and the total number of cells positive for IFN-γ were displayed as an individual value plot. (*E*) The total number of cells positive for either CD4 or CD8 and T cell exhaustion marker PD-1 from the tumors of PBS- and XP-524–treated mice. (*F*) Tumor-infiltrating T cells were gated based on CD4 staining and analyzed for CD25 and FoxP3, and the total number of CD4+CD25+FoxP3 Tregs were displayed as individual value plot. (*G* and *H*) Panc1 cells were treated with either a DMSO vehicle or 1 μM XP-524, analyzed by RNA sequencing, and subjected to GSEA revealing a significant enrichment for the antigen-processing and presentation pathway. (*I*) Tissues from KPC mice treated with either PBS or XP-524 were stained via IHC for MHC Class 1 and representative images displayed. (*J* and *K*) RNA sequencing and GSEA for Panc1 treated as described, revealing a significant down-regulation of the TGFβ signaling pathway. (*L*) Homogenized tumor tissue or serum from KPC mice treated with either PBS or XP-524 were analyzed for levels of TGFβ1 by ELISA.

intratumoral and serum levels of TGFβ1 (Fig. 6*L*), also consistent with diminished peripheral tolerance.

XP-524 Cooperates with PD-1 Inhibition to Further Extend Survival in KPC Mice. Given the enhanced infiltration of functionally exhausted T cells in KPC mice treated with XP-524, as well as the observations that XP-524 increases antigen presentation and diminishes immunosuppressive TGFβ signaling, we next explored the combination of XP-524 with anti–PD-1 in vivo. KPC mice were again allowed to develop overt PDAC for a minimum of 14 wk and randomized at a 50:50 male to female ratio into one of two treatment groups ($n = 7$ per group). Mice were administered either a fixed, 200-μg dose of anti–PD-1 every other day and/or daily IP injections of 5 mg/kg XP-524 (Fig. 7*A*). While anti–PD-1 had no significant effect on survival, the combination of XP-524 and anti–PD-1 significantly improved survival, exceeding that observed with XP-524 alone. In contrast to the 51-d median survival observed with anti–PD-1 alone, mice treated with both XP-524 and anti–PD-1 had a median survival of 161-d postenrollment (Fig. 7*B*). Tissues were again collected at the study end point, revealing a robust CD45+ infiltrate, paralleled by increased CD3+ T cells (Fig. 7 *C*–*E*). Additionally, we observed a highly significant increase in CD8+ T cells and the deposition of granzymeB in remaining areas of disease accompanied by increased apoptosis (Fig. 7*F*).

We next repeated this experiment, enrolling KPC mice as described and treating with either anti–PD-1 or XP-524 and anti–PD-1 for 2 mo. At the study end point, the pancreata and spleens from anti–PD-1– or XP-524–treated mice ($n = 4$ per group) were subjected to flow cytometry as described previously. While anti–PD-1 modestly increased the presence of tumor-infiltrating T cells, mice treated with both drugs had enhanced infiltration of CD4+ and CD8+ T cells, well-surpassing that induced by XP-524 alone (Fig. 7*G*). However, unlike T cells from mice treated with only XP-524, CD8+ T cells were largely positive for IFNγ, and both CD4+ and CD8+ populations had low levels of the exhaustion marker PD-1 (Fig. 7 *H* and *I*). As with XP-524 monotherapy, KPC mice treated with XP-524 and anti–PD-1 had a reduced frequency of intratumoral Tregs, CD4+CD25+FoxP3+ regulatory Tregs, with no change in splenic Tregs (Fig. 7*J* and *SI Appendix*, Fig. S4*A*). The combination of XP-524 and anti–PD-1 led to a substantial increase in tumor infiltration of CD45+CD11b+GR-1+ macrophages, though a reduction in the percent of macrophages positive for the M2 marker CD206 (*SI Appendix*, Fig. S4*B*).

Consistent with an increase in cell-mediated cytotoxicity and reduction in T cell exhaustion, the combination of XP-524 and anti–PD-1 enhanced expression of the surrogate marker of cytotoxicity perforin-1 in tumor-infiltrating CD8+ T cells, though no significant change was observed in splenic CD8+ T cells (Fig. 7*K*). These perforin-1–expressing CD8+ T cells were also highly positive for the activation marker IFNγ, confirming the reduction in peripheral tolerance and increase in antitumor immune function following treatment with XP-524 and anti–PD-1 (Fig. 7*L*).

Discussion

There are currently no curative therapies for patients with advanced PDAC. While broad-spectrum chemotherapy can modestly extend survival, nearly all patients will eventually progress on treatment, and overall outcomes remain poor (34). Additionally, PDAC has shown poor clinical responses to newly emerging treatments, including immunotherapy, in clinical trials (35, 36). Several molecular-based therapies have been suggested to potentiate or replace first-line chemotherapy for PDAC, with BET inhibitors showing particular promise in preclinical studies (4, 5, 7, 37, 38). Based on these results and the established tumor-permissive role of the BET protein BRD4, we developed XP-524, a dual-specificity inhibitor of BRD4, and its upstream HAT EP300. Unlike conventional BET inhibitors, XP-524 completely disrupted the protein–protein interaction between EP300 and BRD4, an interaction that is important in chromatin structure and active transcription (39), and suppressed the acetylation of H3K27, a known action of EP300 (40). Consistent with these observations, XP-524 showed superior potency than the first-generation BET inhibitor JQ-1 and similar efficacy to high-dose JQ-1 combined with EP300 inhibition. Subsequent, RNA-sequencing analysis revealed that concomitant BET and EP300 inhibition, either through combined JQ-1 and SGC-CBP30 or single-agent XP-524, led to a significant down-regulation of KRAS mRNA, with a corresponding decrease in protein expression.

KRAS mutations are observed in over 90% of PDAC patients, resulting in permanent activation of the KRAS protein, which drives several cancer-associated cellular processes, including proliferation, transformation, invasion, and survival (41–44). Oncogenic KRAS mutations have long been considered an early event in PDAC etiology, and sustained KRAS activity is required for both the initiation and maintenance of the neoplastic phenotype (45). Despite the well-established role of oncogenic KRAS in PDAC, KRAS has proven largely undruggable in the clinic (46), with the notable exception of the 1% of PDAC patients with a $KRAS^{G12C}$ mutation where the small molecule inhibitor AMG 510 is showing early promise (47). While most therapies directed against KRAS have sought to directly interfere with the KRAS protein directly (46), we found that concomitant BRD4 and EP300 inhibition impedes KRAS transcription and restrains its downstream signaling.

The cellular mechanisms that direct KRAS expression in PDAC are poorly understood. While our results suggest that cooperation between EP300 and BRD4 is required for KRAS expression, BET proteins are classically associated with MYC signaling and not necessarily KRAS (10). Hence, these results raise several important questions regarding the role of post-translational histone modification and BET proteins in KRAS expression and potentially offer a strategy to subvert the effects of oncogenic KRAS in the clinic. While the mechanistic link between BET proteins and KRAS expression requires further exploration, several studies have suggested that KRAS-mutated tumors are amenable to BET inhibition. For example, JQ-1 has shown significant preclinical efficacy in KRAS-mutated lung tumors (48), as did the combination of JQ-1 and the HDAC inhibitor SAHA in KRAS-driven PDAC (4).

Though encouraging, it is important to note that BET inhibitors are still emerging in the clinic. To date, most clinical data on small molecule BET inhibitors are limited to early-phase trials of patients with either hematologic malignancies or pan-cancer studies in solid tumors (49). The vast majority of BET inhibitors in clinical development are oral, small-molecule inhibitors that interact with the acetylated lysine histone tail–binding pocket, preventing BET protein interaction with its transcription factor partners (49). While BET protein degraders are in preclinical development, these have yet to reach clinical trial (50). Hence, though BET proteins such as BRD4 are known to drive pancreatic cancer progression, clinical progress for BET inhibitors in cancer has been difficult. For instance, a phase IIb trial in midline nuclear protein in testis (NUT) carcinoma evaluating the BET inhibitor MK-8628 (formerly OTX015) was closed because of a lack of detectable clinical activity (NCT02296476). Similarly, the BET inhibitor BAY1238097 went to trial in several solid tumors, though this was terminated because of the high rates of dose-limiting toxicities at subtherapeutic doses (51). Additionally, the selective BET inhibitor GSK525762 is under investigation in NUT midline carcinoma and other solid cancers and to date has only shown partial responses in 2 out of 10 patients with high

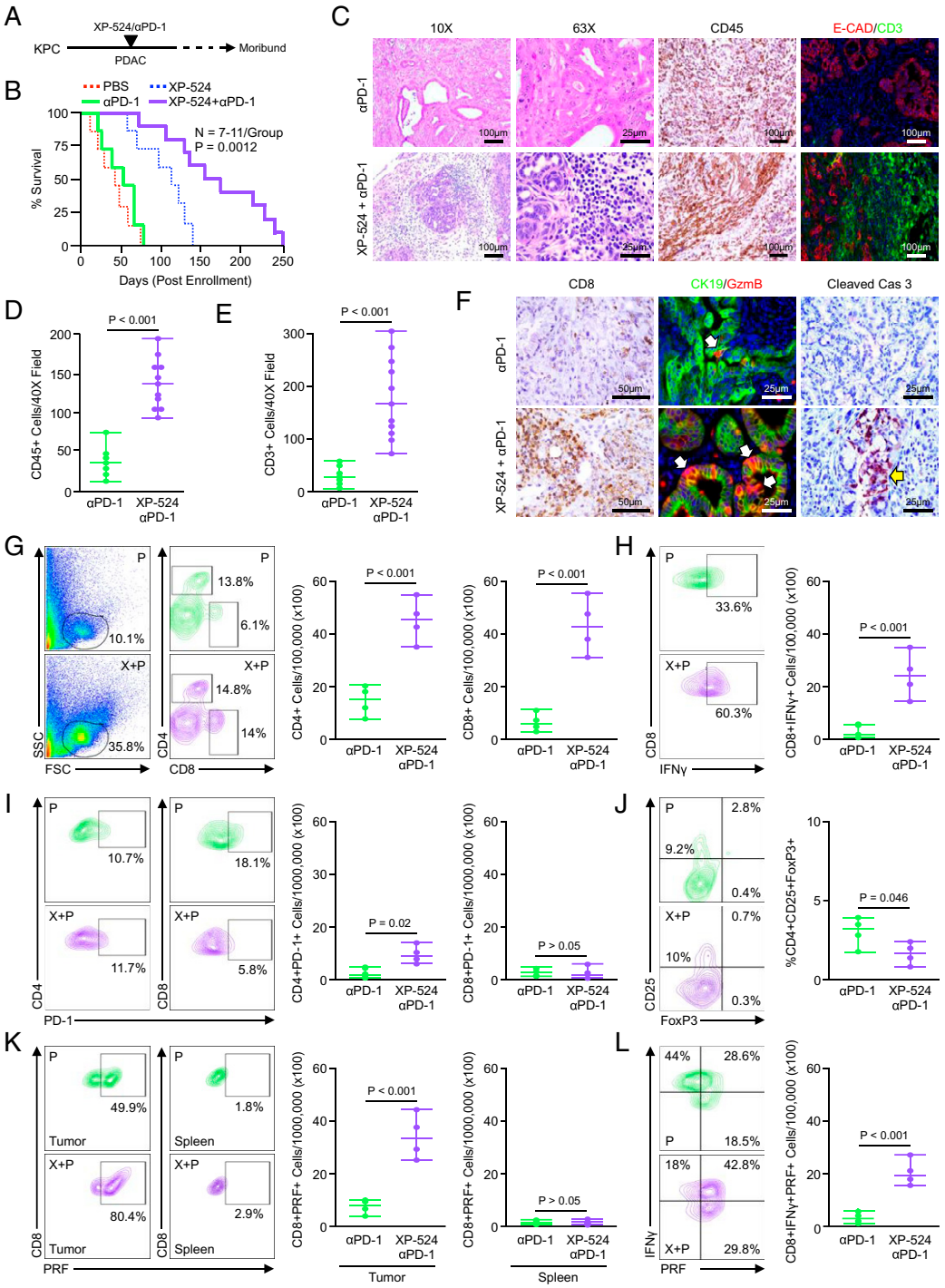

Fig. 7. XP-524 cooperates with PD-1 inhibition to further extend survival in KPC mice. (*A*) KPC mice were generated as a model of advanced PDAC. Starting at 15 wk of age, mice were administered either twice weekly IP injections of 200 μg anti–PD-1 ($n = 7$) or daily injections of 5 mg/kg XP-524 with twice weekly injections of anti–PD-1 ($n = 11$). The study was concluded when animals showed signs of disease-associated morbidity. (*B*) Kaplan–Meier curve indicating survival for mice across both groups in days postenrollment. (*C–E*) At the study end point, pancreas tissues were collected and stained with either H&E or via IHC for pan-leukocyte marker CD45 or for E-cadherin and the T cell surrogate CD3. Tissues were quantified as described and counts displayed as individual value plots. (*F*) Tumor tissues were also stained for the cytotoxic T cell marker CD8, CK19, and granzymeB or the apoptosis surrogate cleaved caspase 3. (*G*) KPC mice were enrolled as described and treated with either anti–PD-1 or XP-524 and anti–PD-1. After 2 mo on treatment, tumor tissues were collected and analyzed by flow cytometry for tumor-infiltrating CD4+ and CD8+ T cells, respectively ($n = 4$ per group). FSC, forward scatter; SSC, side scatter. (*H*) Tumor-infiltrating cells were gated based on the CD8 staining shown previously, and the total number of cells positive for IFNγ was displayed as an individual value plot. (*I*) The total number of cells positive for either CD4 or CD8 and T cell exhaustion marker PD-1 from the tumors of anti–PD-1– and XP-524+anti–PD-1–treated mice. (*J*) Tumor-infiltrating T cells were gated based on CD4 staining and analyzed for CD25 and FoxP3, and the total number of CD4+CD25+FoxP3 Tregs was displayed as individual value plot. (*K*) Spleens and tumor-infiltrating cells were gated based on the CD8 and CD4 staining shown above, and CD8+ events were isolated and analyzed for expression of cytotoxic T cell activation marker Perforin (PRF). The total numbers of cells positive for both CD8 and PRF are displayed as individual value plots. (*L*) Tumor-infiltrating CD8+ cells were gated, as previously, and analyzed for the simultaneous expression of the aforementioned T cell activation markers, including perforin and IFNγ. The number of CD8+perforin+IFNγ+ cells from each group is displayed as an individual value plot.

rates of adverse effects, including thrombocytopenia (44%) and nausea (40%) (52).

High rates of toxicity have been observed with nearly all small-molecule BET inhibitors. The most common grade 3/4 and dose-limiting toxicity has been thrombocytopenia, observed in up to 37% of patients. This appears to be a class effect likely due to BRD3 inhibition, which is an important regulator of GATA1-mediated hematopoiesis (53). Thrombocytopenia associated with BET inhibition is reversible and infrequently associated with significant bleeding. Other frequent grade 3/4 and dose-limiting toxicities include diarrhea, nausea/vomiting, anorexia, anemia, and hepatic enzyme abnormalities. Most agents have required dose modifications or use of noncontinuous dosing to improve their side effect profiles (NCT02516553) (54, 55), with the notable exception of RVX000222, which is showing an improved safety threshold (56). Hence, while the substantial efficacy of XP-524 is encouraging, translating these findings to the clinic will require careful evaluation of any potential adverse effects. While our previous observations suggest that XP-524 does reduce platelets in the rat model of thrombocytopenia, the risk of other off-target effects cannot be ignored (23).

Importantly, clinical data also suggest that single-agent BET inhibition may have limited utility in solid tumors, even with a favorable safety profile. While the added effect of EP300 inhibition likely explains the increased efficacy seen with XP-524 compared to JQ-1, it is important to note that all tumor-bearing mice treated with XP-524 eventually succumbed to their disease, and the clinical utility of single-agent XP-524 may similarly be limited. Hence, while XP-524 may prolong survival in early and advanced PDAC, this is likely by inducing a period of temporary tumor stasis or modestly delayed growth, as tumors reached a similar end point over a longer period of time. While BET inhibitors are showing particular promise when combined with gemcitabine (37) or PARP inhibitors (38), we noted that tumors from mice treated with XP-524 displayed an increased presence in both CD4+ and CD8+ T cell populations. However, despite the increase in T cell infiltration, both had a substantial increase in PD-1 expression, a functional marker of T cell exhaustion associated with an inability to mount an antitumor immune response (57).

There are several clinically useful immune checkpoint inhibitors designed to reinvigorate functionally exhausted T lymphocytes and restore the antitumor immune program. However, despite the rapid progress for immune checkpoint inhibition for several cancer histologies (58–64), immunotherapy has yet to show significant efficacy in PDAC (36). There are several barriers to the efficacy of immune checkpoint inhibitors in PDAC, namely, a paucity of antigen presentation and a highly suppressive tumor microenvironment (24, 25, 65, 66). In addition to enhancing the recruitment of T lymphocytes, XP-524 similarly altered a variety of immune processes, namely enhancing antigen presentation and repressing TGFβ signals. TGFβ is emerging as a key mediator of immune suppression within the pancreatic tumor microenvironment (67), and the inhibition of TGFβ signals has shown early promise as an adjuvant to immune checkpoint inhibition in PDAC (24, 25). We, therefore, combined XP-524 with anti–PD-1 in vivo, which effectively restored a cytotoxic immune response and extended survival well beyond XP-524 alone.

BET inhibitors are beginning to show early promise as an adjuvant to immune checkpoint inhibition in other cancers, in part through BET inhibition–mediated silencing of PD-L1 (68–70). The combination of JQ-1 and anti–PD-1 led to a robust immune response and enhanced survival in transgenic models of KRAS-driven, nonsmall cell lung carcinoma (71). Additionally, this same combination led to partial immune responses in xenograft models of PDAC (72). Hence, XP-524 may offer a clinically useful strategy to sensitize pancreatic tumors to immune checkpoint inhibition while simultaneously restraining the effects of KRAS-activating mutations. As immune checkpoint inhibitors are not without toxicity (73), given the adverse events seen with other BET inhibitors, this approach warrants extreme caution should they be explored in clinical trials. However, despite these potential hurdles, our data suggest that XP-524 has significant, single-agent efficacy in PDAC and synergizes with immune checkpoint inhibition. Given the lack of therapeutic options for patients with advanced disease, pending a comprehensive safety evaluation, the combination epigenetic modifiers, such as XP-524 and anti–PD-1, warrants consideration in patients with advanced PDAC.

Materials and Methods

For the full materials and methods please see the *SI Appendix*.

Chemicals and Reagents. XP-524 was designed and synthesized as described previously (23). JQ-1 and SGC-CBP30 were purchased from Sigma-Aldrich and reconstituted in sterile PBS at a stock concentration of 10 μM immediately before use.

Antibodies. All antibodies were purchased from established commercial vendors and were verified by the manufacturer for the specific species and applications for which they were used in this manuscript. A full list of all antibodies used as well as the vendor, clone, and product numbers can be found in *SI Appendix*, Table S1.

Statistical Analysis. Data were analyzed by either Student's *t* test, simple linear regression analysis, hazard ratio, or ANOVA fit to a general linear model in Minitab express, the validity of which was tested by adherence to the normality assumption and the fitted plot of the residuals. Results were arranged by the Tukey method and considered significant at $P < 0.05$ unless otherwise noted. Results are presented as either a boxplot showing the median value and all other values arranged into quartiles or as a mean plus SD. For RNA-sequencing data, significance was determined using false discovery rate–adjusted *P* values and data considered significant at $P < 0.05$.

Study Approval. All experiments involving the use of mice were performed following protocols approved by the Institutional Animal Care and Use Committee at the University of Illinois at Chicago. Patient slides were obtained from fully consenting patients in a deidentified manner from the University of Florida following local Institutional Review Board approval.

Patient and Public Involvement Statement. Beyond offering informed, written consent to collect tissues for research purposes as described in *Study Approval*, neither our patients nor the public were involved in this study.

Data Availability. Data have been deposited in Gene Expression Omnibus (GSE192903). All other study data are included in the article and/or *SI Appendix*.

ACKNOWLEDGMENTS. This work was supported by Veterans Affairs Merit Award I01BX004903 and Career Scientist Award IK6 BX004855 to A.R., Chicago Biomedical Consortium Accelerator Award and NIH UL1TR002003 provided via the UICentre to G.R.J.T. and R.X., NIH F30CA236031 and UIC Award for Graduate Research to D.R.P., NIH R01CA242003 and the Joseph and Ann Matella Fund for Pancreatic Cancer Research to J.G.T. and Z.D., and NIH R01CA217907, NIH R21CA255291, and Veterans Affairs Merit Award I01BX002922 to H.G.M. Per the funding policy of the US Department of Veterans Affairs, we are required to state that these contents do not represent the views of the US Department of Veterans Affairs or the US Government.

1. E. Hessmann, S. A. Johnsen, J. T. Siveke, V. Ellenrieder, Epigenetic treatment of pancreatic cancer: Is there a therapeutic perspective on the horizon? *Gut* **66**, 168–179 (2017).
2. A. Stathis, F. Bertoni, BET proteins as targets for anticancer treatment. *Cancer Discov.* **8**, 24–36 (2018).
3. V. Sahai, A. J. Redig, K. A. Collier, F. D. Eckerdt, H. G. Munshi, Targeting BET bromodomain proteins in solid tumors. *Oncotarget* **7**, 53997–54009 (2016).
4. P. K. Mazur *et al.*, Combined inhibition of BET family proteins and histone deacetylases as a potential epigenetics-based therapy for pancreatic ductal adenocarcinoma. *Nat. Med.* **21**, 1163–1171 (2015).

5. V. Sahai *et al.*, BET bromodomain inhibitors block growth of pancreatic cancer cells in three-dimensional collagen. *Mol. Cancer Ther.* **13**, 1907–1917 (2014).
6. T. N. D. Pham *et al.*, Induction of MNK kinase-dependent eIF4E phosphorylation by inhibitors targeting BET proteins limits efficacy of BET inhibitors. *Mol. Cancer Ther.* **18**, 235–244 (2019).
7. K. Kumar *et al.*, BET inhibitors block pancreatic stellate cell collagen I production and attenuate fibrosis in vivo. *JCI Insight* **2**, e88032 (2017).
8. L. Zeng, M. M. Zhou, Bromodomain: An acetyl-lysine binding domain. *FEBS Lett.* **513**, 124–128 (2002).
9. A. C. Belkina, G. V. Denis, BET domain co-regulators in obesity, inflammation and cancer. *Nat. Rev. Cancer* **12**, 465–477 (2012).
10. J. E. Delmore *et al.*, BET bromodomain inhibition as a therapeutic strategy to target c-Myc. *Cell* **146**, 904–917 (2011).
11. J. Lovén *et al.*, Selective inhibition of tumor oncogenes by disruption of super-enhancers. *Cell* **153**, 320–334 (2013).
12. P. Filippakopoulos *et al.*, Selective inhibition of BET bromodomains. *Nature* **468**, 1067–1073 (2010).
13. H. Thomas, Therapy: Targeting chromatin remodelling proteins to treat pancreatic cancer. *Nat. Rev. Gastroenterol. Hepatol.* **12**, 608 (2015).
14. J. Shi, C. R. Vakoc, The mechanisms behind the therapeutic activity of BET bromodomain inhibition. *Mol. Cell* **54**, 728–736 (2014).
15. G. Manzotti, A. Ciarrocchi, V. Sancisi, Inhibition of BET proteins and histone deacetylase (HDACs): Crossing roads in cancer therapy. *Cancers (Basel)* **11**, 304 (2019).
16. C. Dhalluin *et al.*, Structure and ligand of a histone acetyltransferase bromodomain. *Nature* **399**, 491–496 (1999).
17. D. A. Santillan *et al.*, Bromodomain and histone acetyltransferase domain specificities control mixed lineage leukemia phenotype. *Cancer Res.* **66**, 10032–10039 (2006).
18. D. A. Hay *et al.*, Discovery and optimization of small-molecule ligands for the CBP/p300 bromodomains. *J. Am. Chem. Soc.* **136**, 9308–9319 (2014).
19. V. Garcia-Carpizo *et al.*, CREBBP/EP300 bromodomains are critical to sustain the GATA1/MYC regulatory axis in proliferation. *Epigenetics Chromatin* **11**, 30 (2018).
20. A. R. Conery *et al.*, Bromodomain inhibition of the transcriptional coactivators CBP/EP300 as a therapeutic strategy to target the IRF4 network in multiple myeloma. *eLife* **5**, e10483 (2016).
21. Y. Yan *et al.*, The novel BET-CBP/p300 dual inhibitor NEO2734 is active in SPOP mutant and wild-type prostate cancer. *EMBO Mol. Med.* **11**, e10659 (2019).
22. X. Zhang *et al.*, Therapeutic targeting of p300/CBP HAT domain for the treatment of NUT midline carcinoma. *Oncogene* **39**, 4770–4779 (2020).
23. Y. Li *et al.*, Novel pyrrolopyridone bromodomain and extra-terminal motif (BET) inhibitors effective in endocrine-resistant ER+ breast cancer with acquired resistance to fulvestrant and palbociclib. *J. Med. Chem.* **63**, 7186–7210 (2020).
24. D. R. Principe *et al.*, TGFβ blockade augments PD-1 inhibition to promote T-cell-mediated regression of pancreatic cancer. *Mol. Cancer Ther.* **18**, 613–620 (2019).
25. D. R. Principe *et al.*, Long-term gemcitabine treatment reshapes the pancreatic tumor microenvironment and sensitizes murine carcinoma to combination immunotherapy. *Cancer Res.* **80**, 3101–3115 (2020).
26. A. Hammitzsch *et al.*, CBP30, a selective CBP/p300 bromodomain inhibitor, suppresses human Th17 responses. *Proc. Natl. Acad. Sci. U.S.A.* **112**, 10768–10773 (2015).
27. W. A. Cortopassi, K. Kumar, R. S. Paton, Cation-π interactions in CREBBP bromodomain inhibition: An electrostatic model for small-molecule binding affinity and selectivity. *Org. Biomol. Chem.* **14**, 10926–10938 (2016).
28. K. Kumar *et al.*, Cation-π interactions in protein-ligand binding: Theory and data-mining reveal different roles for lysine and arginine. *Chem. Sci.* **9**, 2655–2665 (2018).
29. X. Jiang, Y. D. Seo, K. M. Sullivan, V. G. Pillarisetty, Establishment of slice cultures as a tool to study the cancer immune microenvironment. *Methods Mol. Biol.* **1884**, 283–295 (2019).
30. C. Y. Lim *et al.*, Organotypic slice cultures of pancreatic ductal adenocarcinoma preserve the tumor microenvironment and provide a platform for drug response. *Pancreatology* **18**, 913–927 (2018).
31. C. B. Westphalen, K. P. Olive, Genetically engineered mouse models of pancreatic cancer. *Cancer J.* **18**, 502–510 (2012).
32. B. T. DeCant, D. R. Principe, C. Guerra, M. Pasca di Magliano, P. J. Grippo, Utilizing past and present mouse systems to engineer more relevant pancreatic cancer models. *Front. Physiol.* **5**, 464 (2014).
33. S. R. Hingorani *et al.*, Trp53R172H and KrasG12D cooperate to promote chromosomal instability and widely metastatic pancreatic ductal adenocarcinoma in mice. *Cancer Cell* **7**, 469–483 (2005).
34. R. L. Siegel, K. D. Miller, A. Jemal, Cancer statistics, 2019. *CA Cancer J. Clin.* **69**, 7–34 (2019).
35. P. R. Kunk, T. W. Bauer, C. L. Slingluff, O. E. Rahma, From bench to bedside a comprehensive review of pancreatic cancer immunotherapy. *J. Immunother. Cancer* **4**, 14 (2016).
36. D. R. Principe, M. Korc, S. D. Kamath, H. G. Munshi, A. Rana, Trials and tribulations of pancreatic cancer immunotherapy. *Cancer Lett.* **504**, 1–14 (2021).
37. F. Xie *et al.*, The BET inhibitor I-BET762 inhibits pancreatic ductal adenocarcinoma cell proliferation and enhances the therapeutic effect of gemcitabine. *Sci. Rep.* **8**, 8102 (2018).
38. A. L. Miller *et al.*, The BET inhibitor JQ1 attenuates double-strand break repair and sensitizes models of pancreatic ductal adenocarcinoma to PARP inhibitors. *EBioMedicine* **44**, 419–430 (2019).
39. T. Wu, Y. F. Kamikawa, M. E. Donohoe, Brd4's bromodomains mediate histone H3 acetylation and chromatin remodeling in pluripotent cells through P300 and Brg1. *Cell Rep.* **25**, 1756–1771 (2018).
40. H. Ono *et al.*, C646 inhibits G2/M cell cycle-related proteins and potentiates antitumor effects in pancreatic cancer. *Sci. Rep.* **11**, 10078 (2021).
41. L. Buscail, B. Bournet, P. Cordelier, Role of oncogenic KRAS in the diagnosis, prognosis and treatment of pancreatic cancer. *Nat. Rev. Gastroenterol. Hepatol.* **17**, 153–168 (2020).
42. M. P. di Magliano, C. D. Logsdon, Roles for KRAS in pancreatic tumor development and progression. *Gastroenterology* **144**, 1220–1229 (2013).
43. V. T. Smit *et al.*, KRAS codon 12 mutations occur very frequently in pancreatic adenocarcinomas. *Nucleic Acids Res.* **16**, 7773–7782 (1988).
44. C. Almoguera *et al.*, Most human carcinomas of the exocrine pancreas contain mutant c-K-ras genes. *Cell* **53**, 549–554 (1988).
45. M. A. Collins *et al.*, Oncogenic Kras is required for both the initiation and maintenance of pancreatic cancer in mice. *J. Clin. Invest.* **122**, 639–653 (2012).
46. P. Liu, Y. Wang, X. Li, Targeting the untargetable KRAS in cancer therapy. *Acta Pharm. Sin. B* **9**, 871–879 (2019).
47. D. S. Hong *et al.*, CodeBreak 100: Phase I study of AMG 510, a novel KRASG12C inhibitor, in patients (pts) with advanced solid tumors other than non-small cell lung cancer (NSCLC) and colorectal cancer (CRC). *J. Clin. Oncol.* **38**, 3511 (2020).
48. T. Shimamura *et al.*, Efficacy of BET bromodomain inhibition in Kras-mutant non-small cell lung cancer. *Clin. Cancer Res.* **19**, 6183–6192 (2013).
49. S. A. Piha-Paul *et al.*, First-in-human study of mivebresib (ABBV-075), an oral pan-inhibitor of bromodomain and extra terminal proteins, in patients with relapsed/refractory solid tumors. *Clin. Cancer Res.* **25**, 6309–6319 (2019).
50. K. Raina *et al.*, PROTAC-induced BET protein degradation as a therapy for castration-resistant prostate cancer. *Proc. Natl. Acad. Sci. U.S.A.* **113**, 7124–7129 (2016).
51. S. Postel-Vinay *et al.*, First-in-human phase I study of the bromodomain and extraterminal motif inhibitor BAY 1238097: Emerging pharmacokinetic/pharmacodynamic relationship and early termination due to unexpected toxicity. *Eur. J. Cancer* **109**, 103–110 (2019).
52. P. J. O'Dwyer *et al.*, Abstract CT014: GSK525762, a selective bromodomain (BRD) and extra terminal protein (BET) inhibitor: Results from part 1 of a phase I/II open-label single-agent study in patients with NUT midline carcinoma (NMC) and other cancers. *Cancer Res.* **76**, CT014 (2016).
53. A. J. Stonestrom *et al.*, Functions of BET proteins in erythroid gene expression. *Blood* **125**, 2825–2834 (2015).
54. S. A. Piha-Paul *et al.*, Phase 1 study of molibresib (GSK525762), a bromodomain and extra-terminal domain protein inhibitor, in NUT carcinoma and other solid tumors. *JNCI Cancer Spectr.* **4**, pkz093 (2019).
55. J. Lewin *et al.*, Phase Ib trial with birabresib, a small-molecule inhibitor of bromodomain and extraterminal proteins, in patients with selected advanced solid tumors. *J. Clin. Oncol.* **36**, 3007–3014 (2018).
56. S. J. Nicholls *et al.*, Efficacy and safety of a novel oral inducer of apolipoprotein a-I synthesis in statin-treated patients with stable coronary artery disease a randomized controlled trial. *J. Am. Coll. Cardiol.* **57**, 1111–1119 (2011).
57. Y. Jiang, Y. Li, B. Zhu, T-cell exhaustion in the tumor microenvironment. *Cell Death Dis.* **6**, e1792 (2015).
58. F. S. Hodi *et al.*, Improved survival with ipilimumab in patients with metastatic melanoma. *N. Engl. J. Med.* **363**, 711–723 (2010). Correction in: *N. Engl. J. Med.* **363**, 1290 (2010).
59. C. Robert *et al.*, Ipilimumab plus dacarbazine for previously untreated metastatic melanoma. *N. Engl. J. Med.* **364**, 2517–2526 (2011).
60. H. Borghaei *et al.*, Nivolumab versus docetaxel in advanced nonsquamous non-small-cell lung cancer. *N. Engl. J. Med.* **373**, 1627–1639 (2015).
61. E. B. Garon *et al.*; KEYNOTE-001 Investigators, Pembrolizumab for the treatment of non-small-cell lung cancer. *N. Engl. J. Med.* **372**, 2018–2028 (2015).
62. J. Larkin *et al.*, Combined nivolumab and ipilimumab or monotherapy in untreated melanoma. *N. Engl. J. Med.* **373**, 23–34 (2015). Correction in: *N. Engl. J. Med.* **379**, 2185 (2018).
63. G. T. Gibney, L. M. Weiner, M. B. Atkins, Predictive biomarkers for checkpoint inhibitor-based immunotherapy. *Lancet Oncol.* **17**, e542–e551 (2016).
64. P. Darvin, S. M. Toor, V. Sasidharan Nair, E. Elkord, Immune checkpoint inhibitors: Recent progress and potential biomarkers. *Exp. Mol. Med.* **50**, 1–11 (2018).
65. R. J. Torphy, Y. Zhu, R. D. Schulick, Immunotherapy for pancreatic cancer: Barriers and breakthroughs. *Ann. Gastroenterol. Surg.* **2**, 274–281 (2018).
66. J. Zhao *et al.*, Irreversible electroporation reverses resistance to immune checkpoint blockade in pancreatic cancer. *Nat. Commun.* **10**, 899 (2019).
67. D. R. Principe *et al.*, TGFβ signaling in the pancreatic tumor microenvironment promotes fibrosis and immune evasion to facilitate tumorigenesis. *Cancer Res.* **76**, 2525–2539 (2016).
68. H. Zhu *et al.*, BET bromodomain inhibition promotes anti-tumor immunity by suppressing PD-L1 expression. *Cell Rep.* **16**, 2829–2837 (2016).
69. S. J. Hogg *et al.*, BET-bromodomain inhibitors engage the host immune system and regulate expression of the immune checkpoint ligand PD-L1. *Cell Rep.* **18**, 2162–2174 (2017).
70. K. Ebine *et al.*, Interplay between interferon regulatory factor 1 and BRD4 in the regulation of PD-L1 in pancreatic stellate cells. *Sci. Rep.* **8**, 13225 (2018).
71. D. O. Adeegbe *et al.*, BET bromodomain inhibition cooperates with PD-1 blockade to facilitate antitumor response in *Kras*-mutant non-small cell lung cancer. *Cancer Immunol. Res.* **6**, 1234–1245 (2018).
72. Y. Pan *et al.*, Synergistic inhibition of pancreatic cancer with anti-PD-L1 and c-Myc inhibitor JQ1. *OncoImmunology* **8**, e1581529 (2019).
73. J. A. Marin-Acevedo, R. M. Chirila, R. S. Dronca, Immune checkpoint inhibitor toxicities. *Mayo Clin. Proc.* **94**, 1321–1329 (2019).